J. Fluid Mech. (1977), *vol.* 80, *part* 2, *pp.* 259–278
Printed in Great Britain

A porous prolate-spheroidal model for ciliated micro-organisms

By STUART R. KELLER† AND THEODORE Y. WU
Department of Engineering Science, California Institute of Technology, Pasadena

(Received 5 April 1976)

A fluid-mechanical model is developed for representing the mechanism of propulsion of a finite ciliated micro-organism having a prolate-spheroidal shape. The basic concept is the representation of the micro-organism by a prolate-spheroidal control surface upon which certain boundary conditions on the tangential and normal fluid velocities are prescribed. Expressions are obtained for the velocity of propulsion, the rate of energy dissipation in the fluid exterior to the cilia layer, and the stream function of the motion. The effect of the shape of the organism upon its locomotion is explored. Experimental streak photographs of the flow around both freely swimming and inert sedimenting *Paramecia* are presented and good agreement with the theoretical prediction of the streamlines is found.

1. Introduction

The manner in which various micro-organisms propel themselves, while captivating micro-biologists for centuries, has only recently attracted the attention of hydrodynamicists. Although micro-organisms move in many fascinating ways, there are two predominant types of locomotion which taxonomists have long used as a basis for classification. Flagellates consist of a head and one or more long slender motile organelles called flagella. In almost all cases they move by propagating a wave or bend along their flagellum in a direction opposite to that of the overall mean motion. Ciliates, on the other hand, consist of a body that is covered by a great number of hair-like organelles called cilia. They move as a result of the individual cilia beating in concert.

Since micro-organisms are minute in size, the Reynolds number, based upon a certain characteristic dimension of the body l and the speed of propulsion U, is very small, i.e. $R_e = Ul/\nu \ll 1$, ν being the kinematic viscosity of the liquid medium. For the motion of most protozoa, the Reynolds number is of the order of 10^{-2} or less. Hence the predominant forces acting on micro-organisms are viscous forces, the inertia forces being negligible. This fact prompted Taylor (1951) to pose the question

> How can a body propel itself when the inertia forces, which are the essential element in self-propulsion of all large living or mechanical bodies, are small compared with the forces due to viscosity?

† Present address: Department of Civil Engineering and Engineering Mechanics, Columbia University, New York 10027.

In attempting to answer Taylor's question, most fluid-mechanical research on cell motility has so far been on flagellated micro-organisms. This is probably because they are the easier system to model theoretically. The inert head creates a drag while the beating flagellum provides a thrust, and the condition that the thrust must balance the drag yields a relation between the speed of propulsion and the other fluid-dynamical parameters of the motion. Hydrodynamic models for ciliated micro-organisms, on the other hand, are necessarily more complex than those for flagellates because the thrust and drag cannot be separated in considerations of the momentum balance. In contrast to the fluid-mechanical research, however, most biological research on protozoa, in which motility is often used as an assay of internal cell functions, has been devoted to the ciliates. This is principally because they are easier to obtain and to maintain in the laboratory than the flagellates.

Primarily owing to the great complexity of ciliary movement, existing theoretical models for predicting the motion of ciliates fall considerably short of adequately representing the physical phenomena. Several authors, including Blake (1971*b*, 1972), Brennen (1974) and Keller, Wu & Brennen (1975), have considered geometrically simplified models involving planar or cylindrical surfaces of infinite extent. These infinite models have made important contributions to our understanding of several aspects of the problem. However, while these models can be used as local approximations where the ratio of the cilium length to the radius of curvature of the cell surface is small, they are limited in their capacity to assess the effect of the finite three-dimensional shape of the organism upon its locomotion.

There have also been several theoretical investigations of ciliary locomotion using a spherical geometry. Lighthill (1952), Blake (1971*a*) and Brennen (1974) have considered the propulsion of spherically shaped micro-organisms using an envelope model which replaces the organism by a material envelope undergoing small amplitude undulations about a spherical shape. In each of these investigations it is assumed that the fluid adheres to a material envelope covering the cilia (the no-slip condition) and that the envelope propagates small amplitude waves. While this approach has also illuminated certain important features of the phenomena, as pointed out by Blake & Sleigh (1974), the no-slip condition imposed on the flow at the envelope surface and the small amplitude of the waves are assumptions not fully supported by physical observations.

To overcome these limitations, Blake (1973) considered a different approach to a finite model for a spherical ciliated micro-organism. In this approach two regions were considered, one being the cilia layer and the other the exterior flow field. The velocity field for the cilia layer was determined using an infinite-flat-plate model (cf. Blake 1972), while the velocity field for the external region was taken to be the known solution for a translating sphere with both radial and azimuthal surface velocities (cf. Blake 1971*a*). The two velocity fields were then matched at a spherical control surface covering the cilia. Velocity profiles could then be extended from the cilia layer into the exterior field and the propulsion velocity could be determined. While Blake's finite model sheds considerable light for spherically shaped organisms, its validity for the large number of non-spherical shapes found in nature is not entirely clear.

To assess the effect of geometrical shape upon the locomotion of a ciliated micro-organism, the present investigation carries out a theoretical analysis using a prolate-spheroidal body of arbitrary eccentricity. The central concept of the model is the representation of the micro-organism by a porous prolate-spheroidal control surface upon which certain boundary conditions are prescribed on the tangential and normal fluid velocities. The principal advantage of this approach is that the overall effect of the cilia is represented by prescribed boundary conditions on a simple geometrical surface. Furthermore, since it has been shown that the oscillatory velocities created by the cilia decay rapidly with distance from the cell wall (Brennen 1974; Keller *et al.* 1975), only the mean fluid velocities need be considered.

The development of the model proceeds in a manner aimed at understanding the mechanism of propulsion and the effect of the shape of the body on its locomotion. The geometry and boundary conditions are set forth explicitly in § 2. As viscous forces are dominant when compared with inertial forces at the low Reynolds numbers characteristic of micro-organism movement, the hydrodynamic equations of motion may be approximated by the Stokes equations. In § 3 these equations are solved subject to the appropriate boundary conditions. In § 4 the condition that the total force acting on a freely swimming organism must vanish then yields a relation between the speed of propulsion, the parameters that characterize the boundary conditions and the shape of the organism. Using this relation in § 5, we consider the energy expenditure of a ciliated micro-organism. These considerations lead in § 6 to an estimate of the effect of shape upon the power required for the motility of a ciliate. In order to visualize the flow, an expression is obtained in § 7 for the stream function of the flow field and the streamlines are determined and discussed for several cases. Finally, in § 8, several experimental streak photographs of small neutrally buoyant spheres suspended in the fluid around actual micro-organisms are presented. In order to exhibit the drastic difference between the case of a self-propelling micro-organism and that of a dead specimen sedimenting under gravity, streak photographs have been obtained for both types of flow and are compared with their respective theoretically predicted streamlines.

2. Geometry and boundary conditions

Although ciliates have a wide variety of body shapes, a great number of them are approximately axisymmetric and can be suitably represented by a prolate spheroid. Some common examples include *Tetrahymena pyriformis*, *Spirostomum ambiguum*, and *Paramecium multimicronucleatum* (see figure 1, plate 1). The equation describing the prolate spheroidal control surface S which represents the organism is

$$z^2/a^2+\rho^2/b^2 = 1 \quad (\rho^2 = x^2+y^2,\ a \geqslant b), \tag{1}$$

where a is the semi-major axis and b is the semi-minor axis. The focal length $2c$ and eccentricity e are related by

$$c = (a^2-b^2)^{\frac{1}{2}} = ea \quad (0 \leqslant e < 1). \tag{2}$$

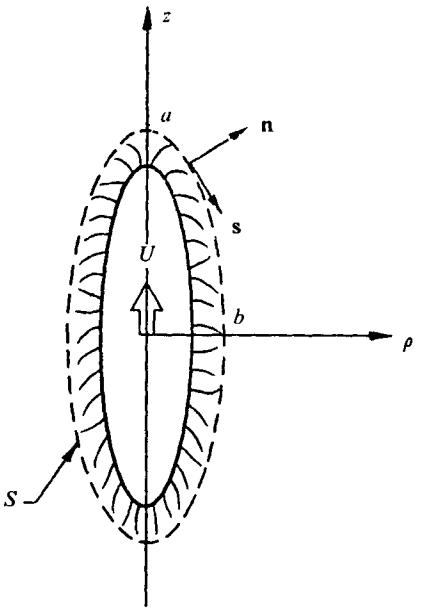

FIGURE 2. The geometry of the model in a meridian plane, illustrating the body of the organism, the cilia layer and the control surface S.

The organism is assumed to be translating with respect to the laboratory frame with velocity $\mathbf{U} = U\mathbf{e}_z$, where $U > 0$ and $\mathbf{e}_z$ is a unit vector pointing in the $+z$ direction. The velocity field with respect to the laboratory frame will be denoted by $\mathbf{u}^l$. The velocity field $\mathbf{u}$ with respect to a co-ordinate system which is fixed with respect to the organism (the body frame) and whose origin and axes coincide with those of the laboratory frame is related to $\mathbf{u}^l$ by

$$\mathbf{u}^l = \mathbf{u} + \mathbf{U}. \tag{3}$$

In this formulation of the problem, the effect of the cilia on the fluid is represented by certain prescribed boundary conditions on the radial component of velocity u_n and on the tangential component of velocity u_s at the control surface S. Axisymmetry about the z axis is assumed. Guided by physical observation and mathematical hindsight, we consider the boundary conditions

$$\mathbf{u} = -U\mathbf{e}_z \quad \text{as} \quad |\mathbf{x}| \to \infty, \tag{4}$$

$$u_n = \mathbf{u}.\mathbf{n} = -V_n(\mathbf{n}.\mathbf{e}_z) \quad \text{on} \quad S, \tag{5}$$

$$u_s = \mathbf{u}.\mathbf{s} = -V_s(\mathbf{s}.\mathbf{e}_z) \quad \text{on} \quad S, \tag{6}$$

where $\mathbf{x}$ is the position vector, the constants V_n and V_s are regarded as parameters of the problem, and $\mathbf{n}$ and $\mathbf{s}$ are unit outward-normal and tangential vectors respectively with the sense of $\mathbf{s}$ indicated in figure 2. It is a simple matter to show that $\mathbf{n}$ and $\mathbf{s}$ are related to $\mathbf{e}_z$ and the unit radial vector $\mathbf{e}_\rho$ by

$$\mathbf{n} = [(1-e^2)^{\frac{1}{2}} z\mathbf{e}_z + (a^2 - z^2)^{\frac{1}{2}} \mathbf{e}_\rho]\,(a^2 - e^2z^2)^{-\frac{1}{2}}, \tag{7}$$

$$\mathbf{s} = [-(a^2 - z^2)^{\frac{1}{2}} \mathbf{e}_z + (1-e^2)^{\frac{1}{2}} z\mathbf{e}_\rho]\,(a^2 - e^2z^2)^{-\frac{1}{2}}. \tag{8}$$

Physically, for $V_n > 0$ and $V_s > 0$, the situation described by (5) and (6) is one in which the lateral cilia impart a tangential slip velocity while fluid is sucked into the cilia layer on the anterior and expelled on the posterior side of the organism. The net flux of fluid into the cilia layer is zero, as it must be by continuity.

These boundary conditions are, of course, far too simple to model accurately the flow produced by any real organism. This possible oversimplification notwithstanding, they were chosen such that a relatively simple solution can be obtained to illustrate the basic mechanism of self-propulsion. We note that, at any point on S, $\mathbf{n}.\mathbf{e}_z = \cos\theta$ and $\mathbf{s}.\mathbf{e}_z = -\sin\theta$, where θ is the angle subtended by $\mathbf{n}$ and $\mathbf{e}_z$. In this sense, (5) and (6) might be viewed as the leading terms in a Fourier expansion in θ of a more general boundary condition.

Physical observations under the microscope suggest that if one were sitting on a swimming organism, one might expect to see, on the average, fluid being sucked into the cilia layer on the front portion of the organism, swept through the cilia layer on the sides, and expelled at the rear. As mentioned above, qualitatively, this is the situation described by (5) and (6). For the purposes of illuminating the overall features of self-propulsion, it is reasonable to expect that the error introduced by not prescribing a more accurate representation of the flow at the control surface will not be large.

3. Solution

The basic equations to be solved are the Stokes equations

$$\nabla p = \mu\nabla^2\mathbf{u}, \quad \nabla.\mathbf{u} = 0, \tag{9), (10}$$

where p is the pressure and μ the coefficient of viscosity, which is taken to be constant. The solution technique employed follows closely the singularity method for Stokes flows lucidly described by Chwang & Wu (1975). We construct the solution by employing a line distribution of Stokeslets and potential doublets between the two foci $z = \pm c$, so that

$$\mathbf{u} = -U\mathbf{e}_z - \int_{-c}^{c} [\alpha\mathbf{U}_S(\mathbf{x}-\boldsymbol{\xi};\,\mathbf{e}_z) - (c^2-\xi^2)\,\beta\mathbf{U}_D(\mathbf{x}-\boldsymbol{\xi};\,\mathbf{e}_z)]\,d\xi, \tag{11}$$

$$p = -\int_{-c}^{c} \alpha P_S(\mathbf{x}-\boldsymbol{\xi};\,\mathbf{e}_z)\,d\xi, \tag{12}$$

where α and β are constants to be determined, $\boldsymbol{\xi} = \xi\mathbf{e}_z$ and

$$\mathbf{U}_S(\mathbf{x}-\boldsymbol{\xi};\,\mathbf{e}_z) = \mathbf{e}_z/R + (\mathbf{e}_z.\mathbf{R})\,\mathbf{R}/R^3 \quad (\mathbf{R} = \mathbf{x}-\boldsymbol{\xi},\ R = |\mathbf{R}|), \tag{13}$$

$$P_S(\mathbf{x}-\boldsymbol{\xi};\,\mathbf{e}_z) = 2\mu\mathbf{e}_z.\mathbf{R}/R^3, \tag{14}$$

$$\mathbf{U}_D(\mathbf{x}-\boldsymbol{\xi};\,\mathbf{e}_z) = -\mathbf{e}_z/R^3 + 3(\mathbf{e}_z.\mathbf{R})\,\mathbf{R}/R^5. \tag{15}$$

The expressions (13) and (14) are the velocity and pressure of a Stokeslet, the fundamental solution of the Stokes equations which is produced by a singular point force

$$\mathbf{f}_s = 8\pi\mu\mathbf{e}_z\,\delta(\mathbf{x}-\boldsymbol{\xi}) \tag{16}$$

acting on the fluid, where $\delta(\mathbf{x}-\boldsymbol{\xi})$ is the three-dimensional Dirac delta function. In (15), $\mathbf{U}_D$ represents the velocity field of a potential doublet, which is also a solution of the Stokes equations and is related to the Stokeslet by $\mathbf{U}_D = \nabla^2\mathbf{U}_s$. Alternatively, $\mathbf{U}_D$ may be derived from the velocity potential

$$\phi_D = -\mathbf{e}_z.\mathbf{R}/R^3. \tag{17}$$

The pressure associated with a potential doublet is zero, in accordance with the present low-Reynolds-number approximation. Equations (11) and (12) represent a linear superposition of the fundamental solutions. By virtue of their construction and the linearity of the problem, they satisfy the Stokes equations (9) and (10) as well as the boundary condition (4) on $\mathbf{u}$ at infinity. The pressure may be gauged, of course, by the addition of an arbitrary constant. The integrated form of (11) and (12) may be written

$$\begin{aligned}\mathbf{u} = &\left\{-U-2(\alpha+\beta)\log\frac{R_2-(z-c)}{R_1-(z+c)}+\alpha\left(\frac{z+c}{R_1}-\frac{z-c}{R_2}\right)\right.\\ &\left.+2\beta c\left(\frac{1}{R_1}+\frac{1}{R_2}\right)\right\}\mathbf{e}_z+\left\{(\alpha+2\beta)\rho\left(\frac{1}{R_1}-\frac{1}{R_2}\right)+\frac{2\beta z}{\rho}\left(\frac{z+c}{R_1}-\frac{z-c}{R_2}\right)\right\}\mathbf{e}_\rho,\end{aligned} \tag{18}$$

$$p = 2\mu\alpha(R_1^{-1}-R_2^{-1}), \tag{19}$$

where

$$R_1 = [(z+c)^2+\rho^2]^{\frac{1}{2}}, \quad R_2 = [(z-c)^2+\rho^2]^{\frac{1}{2}}. \tag{20}$$

To satisfy the boundary conditions (5) and (6), we note that on the control surface S

$$\rho^2 = (1-e^2)(a^2-z^2), \quad R_1 = a+ez, \quad R_2 = a-ez, \tag{21}$$

$$\log\frac{R_2-(z-c)}{R_1-(z+c)} = \log\frac{1+e}{1-e} \equiv L \quad (-a \leqslant z \leqslant a). \tag{22}$$

Consequently (18), when evaluated on the surface S, gives for the surface velocity, after some manipulation,

$$\begin{aligned}\mathbf{u}_0 = &\left[-U-2\alpha L+\beta\left(\frac{4e}{1-e^2}-2L\right)\right](\mathbf{n}.\mathbf{e}_z)\,\mathbf{n}+[-U+2\alpha(e-L)\\ &+2\beta(2e-L)](\mathbf{s}.\mathbf{e}_z)\,\mathbf{s},\end{aligned} \tag{23}$$

where $\mathbf{n}$ and $\mathbf{s}$ are given by (7) and (8). Thus (5) and (6) will be satisfied if

$$\alpha = \frac{e^2}{(1+e^2)L-2e}\left[\frac{1}{1-\kappa}V_n+\frac{1}{1-\kappa^{-1}}V_s-U\right], \tag{24}$$

$$\beta = \frac{1-e^2}{4e^3}[V_s-V_n+2e\alpha], \tag{25}$$

where

$$\kappa = [2e-(1-e^2)L]/[(1-e^2)(2e-L)]. \tag{26}$$

It is noted that, for $V_n = V_s = 0$, (24) and (25) reduce to the results of Chwang & Wu (1975) with U replaced by $-U_1$ for a rigid (no-slip) prolate spheroid translating parallel to its major axis. The above solution may also be derived from the Stokes stream-function equation written in prolate-spheroidal co-ordinates (see Happel & Brenner 1973).

The drag **D** experienced by the organism comes only from the Stokeslets in the solution and may be evaluated simply by superposition to give

$$\mathbf{D} = -8\pi\mu \int_{-c}^{c} (-\alpha \mathbf{e}_z)\, dz = 16\pi\mu c\alpha \mathbf{e}_z. \tag{27}$$

In the limiting case of a sphere ($e \to 0$), (27) becomes

$$\mathbf{D} = -6\pi\mu a[\tfrac{1}{3}(U - V_n) - \tfrac{2}{3}(V_s - U)]\, \mathbf{e}_z, \tag{28}$$

while in the limiting case of a needle ($e \to 1$), (27) reduces to

$$\mathbf{D} = \frac{4\pi\mu a(V_s - U)}{\log(2a/b) - \frac{1}{2}}\, \mathbf{e}_z. \tag{29}$$

Equations (28) and (29) reduce to well-known results for translating rigid (no-slip) bodies when $V_s = V_n = 0$.

4. Self-propulsion

For a freely swimming organism, the total force acting on the body must be zero. From (27) and (24) we see that, in the absence of external forces, this condition will be satisfied if

$$U = \frac{1}{1-\kappa} V_n + \frac{1}{1-\kappa^{-1}} V_s, \tag{30}$$

where κ is given by (26). As e varies from 0 to 1, κ varies from -2 to $-\infty$. Thus it is seen that the normal and tangential components both contribute to the propulsion. If $V_s = 0$, the organism could still propel itself by sucking and expelling fluid across the envelope of the cilia. If $V_n = 0$, the organism could propel itself by creating a slip velocity at the envelope.

The relation between V_n/U and V_s/U for self-propulsion is indicated graphically in figure 3. The curves are a series of straight lines passing through the point ($V_n/U = 1$, $V_s/U = 1$) with slopes which depend on the eccentricity e and which have the limiting value of -2 for $e = 0$ and $-\infty$ for $e = 1$. The point ($V_n/U = 1$, $V_s/U = 1$) corresponds to the situation in which the organism has made itself 'invisible' to the fluid. Indeed for this case $\alpha = \beta = 0$ [see (24) and (25)], and a trivial solution results. It is seen that, in general, for a given speed of propulsion U, the normal velocity V_n necessary for zero drag decreases as the slip velocity V_s increases, and that this effect is enhanced as e goes to 1. Indeed, for V_s/U greater than 1·5, V_n/U must be negative. Physically this means that when V_s/U is large enough the surface integral of the wall shear stress in the $+z$ direction is so great that for equilibrium it is necessary to have the contribution from the normal stress oppose the motion.

It is of interest to investigate the effect of the shape of the organism on its speed of propulsion. In the sphere limit ($e \to 0$), (30) becomes

$$U = \tfrac{1}{3}V_n + \tfrac{2}{3}V_s, \tag{31}$$

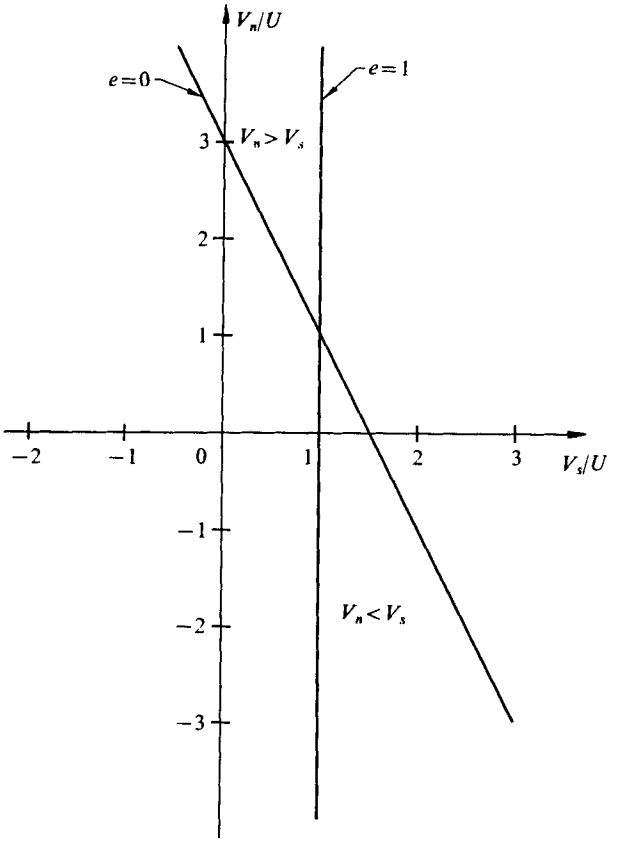

FIGURE 3. The relationship between V_n/U and V_s/U for self-propulsion.

which is in agreement with Blake (1973) with V_s replaced by B_1 and V_n by $-A_1$, while in the needle limit ($e \to 1$) this condition becomes

$$U = V_s. \tag{32}$$

Plots of U/V_s *vs.* e are drawn in figure 4 for various values of V_n/V_s. It is seen that, for $V_n/V_s > 1$, U/V_s decreases with increasing eccentricity, whereas the opposite trend holds for $V_n/V_s < 1$. For most organisms the beat pattern of the cilia is conducive to creating tangential rather than normal velocities, so that we might expect $0 < V_n/V_s < 1$. In this range it may be observed that the speed of propulsion is not altered very much by the shape of the organism. This effect might partially explain why such a wide variety of shapes of ciliated creatures occur in nature.

From (11), (25), and (30) we find that the velocity field for a freely swimming organism ($\alpha = 0$) is

$$(\mathbf{u})_{\alpha=0} = -U\mathbf{e}_z + \beta_0 \int_{-c}^{c} (c^2 - \xi^2)\, \mathbf{U}_D(\mathbf{x} - \boldsymbol{\xi};\, \mathbf{e}_z)\, d\xi, \tag{33}$$

where

$$\beta_0 = (1-e^2)(U - V_n)/2[2e - (1-e^2)L]. \tag{34}$$

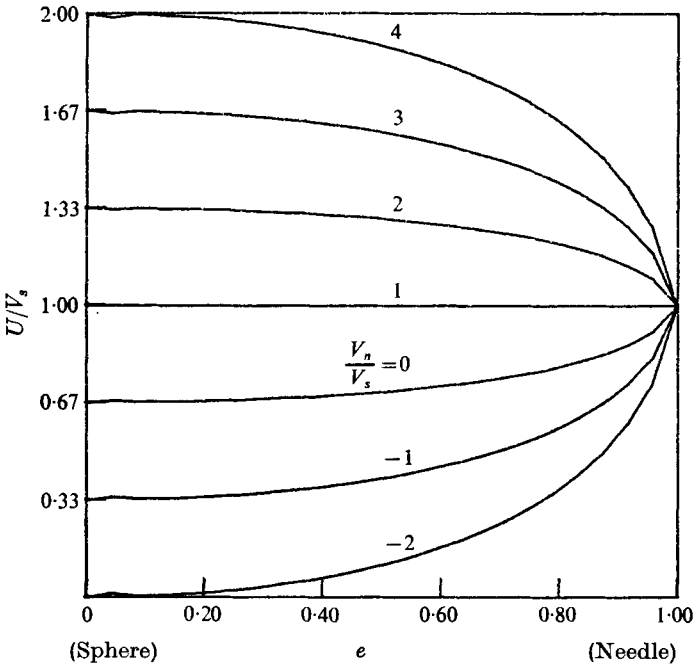

FIGURE 4. Variation of the speed of propulsion U with the eccentricity of the body e. The numbers indicate different values of V_n/V_s, where V_n is the maximum suction velocity and V_s the maximum slip velocity created by the cilia.

It is of interest to note from the work of Chwang & Wu (1974) that the velocity field for the potential flow created by a uniform axial flow $-U\mathbf{e}_z$ past a prolate spheroid of eccentricity e' and focal length c may be represented by

$$\mathbf{u}' = -U\mathbf{e}_z + \beta' \int_{-c}^{c} (c^2 - \xi^2)\, \mathbf{U}_D(\mathbf{x} - \boldsymbol{\xi};\, \mathbf{e}_z)\, d\xi, \tag{35}$$

where

$$\beta' = (1 - e'^2)\, U/2[2e' - (1 - e'^2)\, L'], \tag{36}$$

with $L' = \log[(1+e')/(1-e')]$. Upon comparison of (34) and (36) we see that the velocity field for a swimming prolate-spheroidal-shaped organism of focal length c and eccentricity e is equivalent to the potential flow past a prolate spheroid of the same focal length and eccentricity e' defined by the solution of the transcendental equation

$$\frac{1 - e'^2}{[2e' - (1 - e'^2)\, L']} = \frac{1 - e^2}{[2e - (1 - e^2)\, L]} \left(1 - \frac{V_n}{U}\right). \tag{37}$$

Since the expression on the left-hand side is a decreasing function of e', we see that for $0 < V_n/U < 1$ the equivalent potential-flow prolate spheroid would be more slender.

5. Energy dissipation

As a ciliated micro-organism swims through a fluid, energy is being dissipated by viscosity in the fluid both inside and outside the cilia layer. While an estimate of the former is difficult, the present model allows an evaluation of the latter.

If we regard V as the volume exterior to the control surface S, then it is a well-known result (see, for example, Lamb 1932) that the rate at which energy is being dissipated by viscosity in the fluid occupying V is

$$\dot{E} = -\int_S (\boldsymbol{\sigma}\mathbf{n}).\mathbf{u}^l dS, \tag{38}$$

where $\boldsymbol{\sigma}$ is the Newtonian stress tensor $-p\mathbf{I}+\mu[(\nabla\mathbf{u})+(\nabla\mathbf{u})^{\mathrm{T}}]$, $\mathbf{I}$ being the unit tensor and T indicating a transpose, and $\mathbf{n}$ is the unit outward normal to S as before. By employing (3) we may write (38) as

$$\dot{E} = -\int_S (\boldsymbol{\sigma}\mathbf{n}).\mathbf{u}\, dS - \mathbf{U}\int_S (\boldsymbol{\sigma}\mathbf{n})\, dS. \tag{39}$$

Since the second integral in (39) is just the drag experienced by the body, we may write

$$\dot{E} = -\int_S (\boldsymbol{\sigma}\mathbf{n}).\mathbf{u}\, dS + \mathbf{F}.\mathbf{U}, \tag{40}$$

where $\mathbf{F}$ is the external force equal and opposite to the drag that must be applied to the body in order to maintain such a fluid motion. This equation asserts that the rate at which energy is being dissipated by viscosity is equal to the rate at which work is done by the surface forces at the surface S plus the rate at which work is done by the external force $\mathbf{F}$. We note that, for an impermeable rigid body, $\mathbf{u} = 0$ on S, and so $\dot{E}$ reduces to $\mathbf{F}.\mathbf{U}$. For example, in the fall of a solid sphere the rate of work done by gravity is $6\pi\mu a U^2$, which is the rate of energy dissipation by viscosity.

The evaluation of (38) for the present case is somewhat tedious and the details are given in the appendix. The result is

$$\dot{E} = 8\pi\mu a[(1+e^2)L-2e]\left[\frac{3-e^2}{e}\alpha^2 - 4e\alpha\beta + \frac{4e^3}{1-e^2}\beta^2\right], \tag{41}$$

where α and β are given by (24) and (25) and $L = \log[(1+e)/(1-e)]$ as before. For a freely swimming organism ($\alpha = 0$) it is found from (25), (26), (30) and (41) that the rate of energy expenditure outside the cilia layer is given by

$$\dot{E}_0 = \frac{8\pi\mu a[(1+e^2)L-2e](1-e^2)e^3}{[2e-(1-e^2)L]^2}(U-V_n)^2. \tag{42}$$

For the case of an inert body ($V_n = V_s = 0$), (24), (25) and (41) show that the power required would be

$$\dot{E}_1 = 16\pi\mu a e^3 U^2/[(1+e^2)L-2e]. \tag{43}$$

We see that this expression is in agreement with the expected result that $\dot{E}_1 = -\mathbf{D}.\mathbf{U}$ (cf. (24) and (27) with $V_n = V_s = 0$).

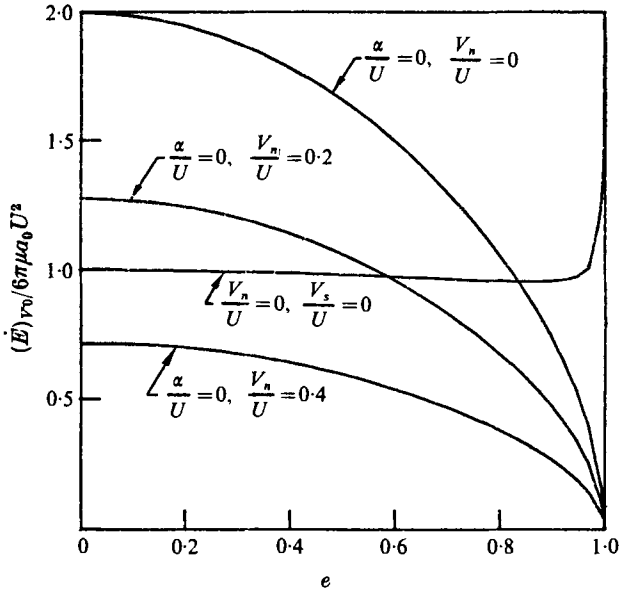

FIGURE 5. Variation of the rate of energy expenditure for a body of constant volume with eccentricity. The energy expenditure rate has been non-dimensionalized by $6\pi\mu a_0 U^2$.

6. The effect of shape upon energy expenditure

A large number of shapes of ciliated micro-organisms occur in nature. For example *Ichthyophthirius multifilis* and *Balantidium coli* are nearly spherical while *Paramecium multimicronucleatum* and *Spirostomum ambiguum* are very slender and elongated. In contrast most fish, while differing in size, have the same general geometrical shape. Furthermore, many individual micro-organisms can alter their shape: *S. ambiguum* can tie itself into a knot.

In the light of the above, it is of interest to investigate the effect of the shape of our model organism, as measured by its eccentricity, upon the rate of energy expenditure. We note that $\dot{E}$ as given by (41) depends upon the length of the major semi-axis of the body a, that is, (41) expresses the rate of energy expenditure for a body of constant length. Physically, however, it is more significant to consider the effect of shape upon a body of constant volume (i.e. mass). In this regard, we note that the volume V_0 of a prolate spheroid is given by

$$V_0 = \tfrac{4}{3}\pi a^3(1-e^2). \tag{44}$$

Therefore for a given V_0, the semi-major axis necessary to maintain a constant volume is

$$a = a_0/(1-e^2)^{\frac{1}{3}}, \tag{45}$$

where $a_0 = (3V_0/4\pi)^{\frac{1}{3}}$. Upon substituting (45) into (41), we obtain for the rate of energy expenditure at constant volume

$$(\dot{E})_{V_0} = \frac{8\pi\mu a_0[(1+e^2)L-2e]}{(1-e^2)^{\frac{1}{3}}}\left[\frac{3-e^2}{e}\alpha^2 - 4e\alpha\beta + \frac{4e^3}{1-e^2}\beta^2\right]. \tag{46}$$

Figure 5 is a plot of $(\dot{E})_{V_0}$, non-dimensionalized by $6\pi\mu a_0 U^2$, against the eccentricity for constant values of V_n/U. The central curve, labelled $V_n/U = 0$, $V_s/U = 0$, corresponds to the translation of an inert impermeable body. Since there is a drag on the body, an external force would be needed to achieve the motion. As the body becomes slender, the drag per unit length diminishes logarithmically [cf. (29)], but the length necessary to maintain a constant volume grows algebraically [cf. (45)]. Thus $(\dot{E})_{V_0}$ is fairly constant until it becomes singular for very high eccentricity.

The other curves correspond to the case of a freely swimming organism ($\alpha = 0$). The tangential velocity component, as previously shown, would vary with eccentricity in order to keep $\alpha = 0$ [cf. (30) or figure 3]. For $V_n/U = 0$, 0·2 and 0·4 it is found that V_s/U varies from 1·5 to 1, 1·4 to 1 and 1·3 to 1 respectively as e goes from 0 to 1. It is seen that for constant V_n/U, $(\dot{E})_{V_0}$ for a freely swimming organism decreases with eccentricity. Furthermore, for constant eccentricity, $(\dot{E})_{V_0}$ decreases for increasing V_n/U within the range $0 < V_n/U < 1$. It is of interest to note that for a sufficiently slender shape (or V_n/U large enough), $(\dot{E})_{V_0}$ is less than the power required to propel an inert impermeable body at the same speed.

In order to compare the energy expenditure within the cilia layer to that outside the cilia layer, we consider a specific organism: *Paramecium multimicronucleatum*. Using simple resistive theory, several authors including Yoneda (1962), Sleigh & Holwill (1969), Hiramoto (1974) and Keller (1975) have estimated the local rate of working of a single cilium. It appears that a conservative estimate of the local rate of working of a single cilium of *P. multimicronucleatum* within the cilia layer would be 1×10^{-7} erg/s. For a typical organism $a = 80\,\mu$m and $b = 30\,\mu$m (cf. figure 1), and the surface density of cilia is about 0·267 cilia/μm^2 (Sleigh 1969). Therefore, if we assume that each cilium works at the same rate, the energy expenditure rate within the cilia layer is about $6{\cdot}7\times10^{-4}$ erg/s. The nominal swimming speed of *P. multimicronucleatum* is observed to be about $2500\,\mu$m/s. Assuming $V_n = 0$, we find from (42) that the energy expenditure rate outside the cilia layer $\dot{E}_0$ is about $3{\cdot}0\times10^{-5}$ erg/s. Therefore we see that for a freely swimming organism most of the power required for motility is expended in the fluid within the cilia layer.

In summary, therefore, the slenderness of the body greatly diminishes the rate of energy spent in the fluid outside the cilia layer. However, since this is probably a small percentage of the energy expended in the fluid within the cilia layer, the efficiency of propulsion would not appear to be greatly altered by the shape of the organism. This conclusion again indicates that this mechanism of propulsion affords an evolutionary advantage.

7. The stream function

In order to visualize the flow field around a micro-organism, we consider the Stokes stream function ψ defined by the equations

$$-\frac{1}{\rho}\frac{\partial\psi}{\partial\rho} = u_z^{\mathrm{II}}, \quad \frac{1}{\rho}\frac{\partial\psi}{\partial z} = u_\rho^{\mathrm{I}}, \tag{47), (48}$$

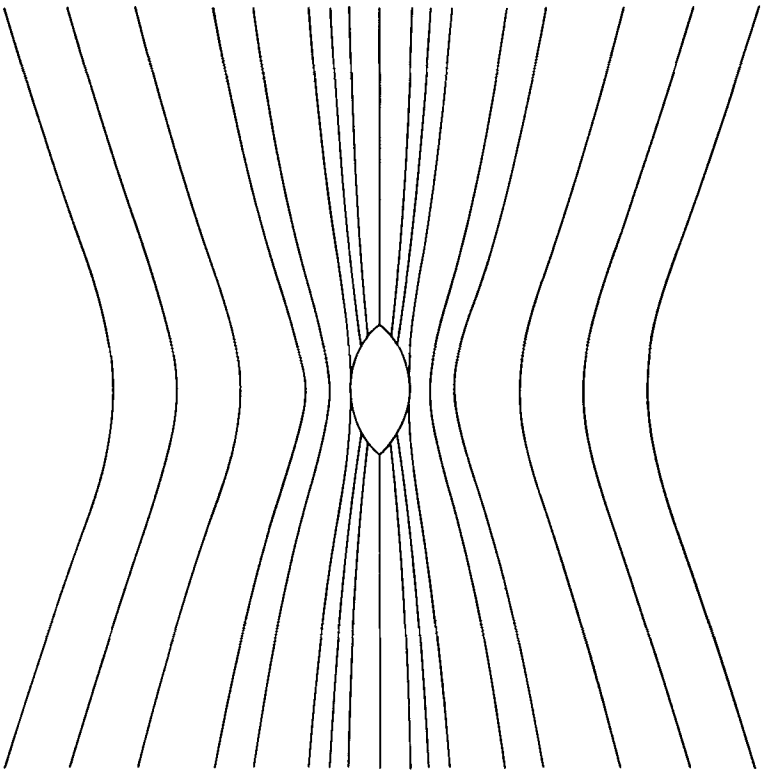

FIGURE 6. The streamlines ψ/c^2U in the laboratory frame for an inert translating prolate spheroid of eccentricity 0·9. Here $V_n/U = V_s/U = 0$.

where $u_\rho^l = \mathbf{u}^l . \mathbf{e}_\rho$ and $u_z^l = \mathbf{u}^l . \mathbf{e}_z$. Making use of the integrated form of $\mathbf{u}$ from (18), we may write (47) and (48) as

$$\frac{\partial\psi}{\partial\rho} = -\rho\left\{-2(\alpha+\beta)\log\frac{R_2-(z-c)}{R_1-(z+c)}+\alpha\left(\frac{z+c}{R_1}-\frac{z-c}{R_2}\right)+2\beta c\left(\frac{1}{R_1}+\frac{1}{R_2}\right)\right\}, \tag{49}$$

$$\frac{\partial\psi}{\partial z} = \rho\left\{(\alpha+2\beta)\rho\left(\frac{1}{R_1}-\frac{1}{R_2}\right)+\frac{2\beta z}{\rho}\left(\frac{z+c}{R_1}-\frac{z-c}{R_2}\right)\right\}, \tag{50}$$

where $R_1 = [(z+c)^2+\rho^2]^{\frac{1}{2}}$ and $R_2 = [(z-c)^2+\rho^2]^{\frac{1}{2}}$ as before. To integrate the first of these, we note that integration by parts yields

$$\int_\rho \log\frac{R_2-(z-c)}{R_1-(z+c)}\,d\rho = \frac{\rho^2}{2}\log\frac{R_2-(z-c)}{R_1-(z+c)}+\tfrac{1}{2}[(z+c)R_1-(z-c)R_2]. \tag{51}$$

Thus integration of (49) yields

$$\psi = (\alpha+\beta)\rho^2\log\frac{R_2-(z-c)}{R_1-(z+c)}+\beta[(z-c)R_1-(z+c)R_2]+f(z), \tag{52}$$

where f is a function of z only. Similarly, integration of (50) yields

$$\psi = (\alpha+\beta)\rho^2\log\frac{R_2-(z-c)}{R_1-(z+c)}+\beta[(z-c)R_1-(z+c)R_2]+g(\rho), \tag{53}$$

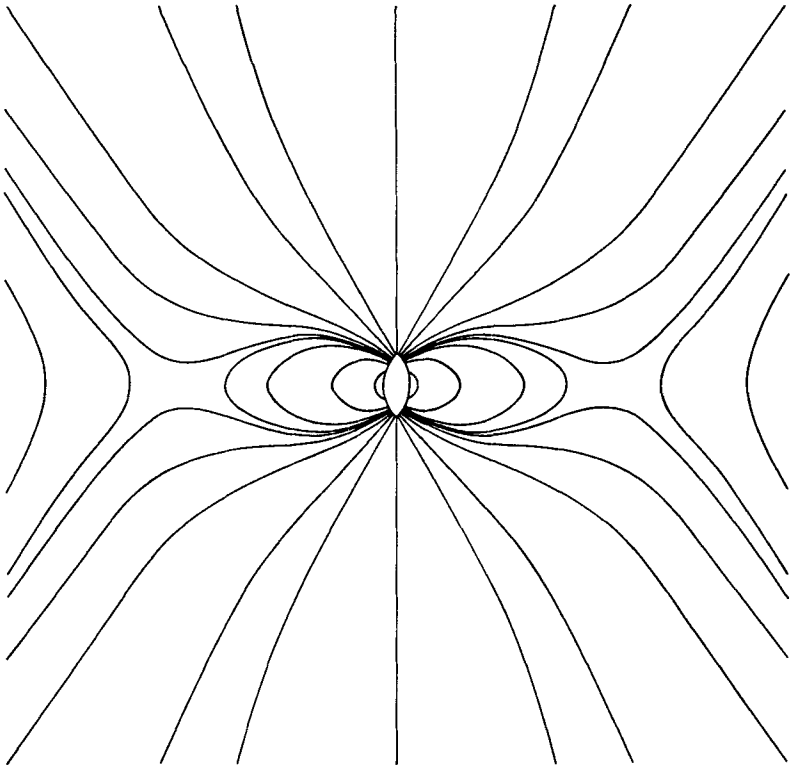

FIGURE 7. The streamlines ψ/c^2U in the laboratory frame for a prolate spheroid having eccentricity 0·9 for the case $V_n/U = 0$, $V_s/U = 1{\cdot}17$.

where g is a function of ρ only. Comparing (52) and (53) we see that

$$f(z) = g(\rho) = \psi_0, \tag{54}$$

where ψ_0 is a constant. Without loss of generality we may take $\psi_0 = 0$. Thus the stream function corresponding to the solution of the problem is

$$\psi = (\alpha+\beta)\rho^2 \log \frac{R_2-(z-c)}{R_1-(z+c)} + \beta[(z-c)R_1-(z+c)R_2], \tag{55}$$

where α and β are given by (24) and (25). Once α and β have been determined by specifying U, V_n, V_s and e [see (24) and (25)], the streamlines in any meridian plane may be found from (55).

In order to illustrate the difference in the streamlines in going from a translating inert impermeable body to a self-propelling organism, we consider the streamlines in the laboratory frame about a prolate spheroid of eccentricity equal to 0·9 for three different cases. In case I we consider a translating inert (no-slip) body specified by $V_n/U = 0$ and $V_s/U = 0$. Equations (24) and (25) imply that $\alpha/U = -0{\cdot}229$ and $\beta/U = -0{\cdot}027$. Again in order to achieve such a flow, an external force must act on the body in order to compensate for the drag, which is given by (27). The streamlines, which are plotted in figure 6, are open in the sense

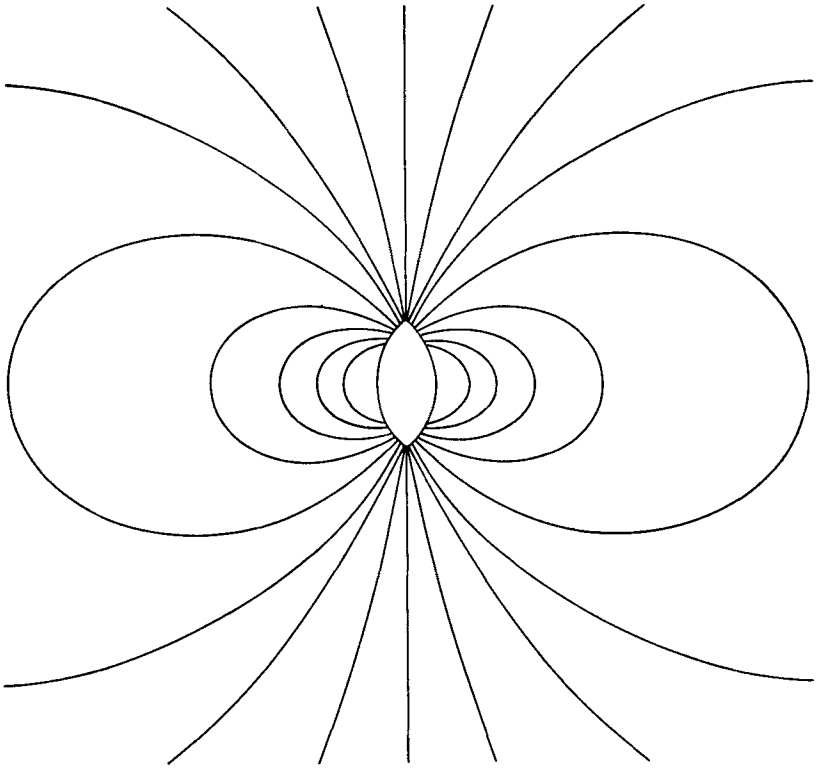

FIGURE 8. The streamlines $\psi/c^2\beta$ in the laboratory frame for a self-propelling prolate-spheroidal body.

that they terminate at infinity. They are similar to the pattern for a sphere (see, for example, Lamb 1932).

In case II we consider an organism for which $V_n/U = 0$ and $V_s/U = 1{\cdot}17$. Equations (24) and (25) now imply that $\alpha/U = -0{\cdot}001$ and $\beta/U = 0{\cdot}076$, so that such a body would experience a slight drag. The streamlines for this case are plotted in figure 7. Now some of the streamlines have two branches, one of which is closed.

Finally in case III we consider a freely swimming organism for which $\alpha/U = 0$ and thus $\mathbf{D} = 0$ [see (27)]. As β now becomes simply a multiplicative factor in (55), the streamlines have the same form for any set of U, V_n, V_s and e satisfying (30). The streamlines shown in figure 8 are all closed except for the trivial one given by $\rho = 0$.

8. Streak photographs of the flow around *Paramecium*

Since the theoretical model developed in this investigation predicts a great difference in the appearance of the streamlines for an inert body and a freely swimming micro-organism, an attempt has been made to verify the model, at least qualitatively, but means of the visualization of the streamlines around actual micro-organisms.

For this purpose specimens of *Paramecium caudatum* were prepared in an aqueous medium in which neutrally buoyant spheres (of 1 μm diameter) were suspended to serve as tracers of the flow field. A Nikon microscope (model L-ke) was employed to achieve a magnification of 200 and the images were recorded on 35 mm film (Kodak 2475) using a Nikon camera (model F). The illumination was by a strobe (Strobex No. 71B) flashing at 6–24 Hz, and the shutter was left open for $\frac{1}{4}$–2 s, allowing about 2–48 multiple exposures.

Figure 9 (plate 2) is a typical streak photograph of a freely swimming *Paramecium caudatum*. The exposure time was $\frac{1}{2}$ s and the strobe frequency was 24 Hz. The streak paths of the tracer spheres around the micro-organism are seen to be at least qualitatively in agreement with figure 8.

Since *Paramecium caudatum* is slightly denser than water, it was also possible to visualize the streamlines around an inert body propelled by an external force (viz. gravity). This was accomplished by carefully killing the organisms (for which purpose gentle heat is recommended) and by mounting the microscope on its side so as to have the microscopic slide inclined to the horizontal. Figure 10 (plate 3) is a typical streak photograph of a dead *Paramecium caudatum* falling under the influence of gravity. The exposure time was 1·5 s and the strobe frequency was 10 Hz. The organisms fell at about one-tenth their freely swimming speed. Again comparison of the particle paths with figure 6 indicates a qualitative agreement between theory and experiment.

In comparing the photographs with the theoretical streamlines, one should keep in mind that the theory did not take into account the effect of the walls and other flow boundaries that were present in the experiment. The specimen preparations were made using a glass slide and a standard vaseline mount in which the coverslip was supported by a certain thickness of vaseline around its perimeter. Although exact measurements were difficult to obtain, this thickness was several times the length of the organism, and care was taken to focus at the central plane of the preparation.

In this regard we note that the inert sedimenting specimens displayed streamlines that closely resemble the Stokes flow in the near field as opposed to the potential-flow streamlines past a freely swimming body of the same shape. At large distances (more than a few body lengths away) from the inert specimen, however, the streamlines are expected to be significantly modified by the wall effects for at least two reasons. First, since the Stokes flow generated by an external force has a velocity field of much longer range than the corresponding potential flow, we may expect it to be subject to relatively stronger wall corrections. Second, the flow may exhibit features relating to the Hele Shaw effect. According to the Hele Shaw effect, a body whose dimensions are large compared with the thickness between two flat plates will produce the streamlines of a potential flow in the gap when the inertial forces are negligible (see, for example, Batchelor 1967).

9. Concluding remarks

The concept of representing a freely swimming micro-organism by a porous prolate spheroid leads to a reasonably successful model for the mechanism of locomotion. The principal advantage of this approach is that it allows us to incorporate the effect of the cilia into prescribed boundary conditions on a simple geometrical control surface.

With the proposed boundary conditions, which seem to be physically reasonable and which are characterized by only two parameters, several features of the propulsion of a prolate-spheroidal ciliated creature may be ascertained. It is found that, within the typical range of parameter values, the speed of propulsion is fairly insensitive to the eccentricity of the body. Furthermore, while the rate at which energy is expended in the fluid outside the cilia layer diminishes with slenderness, this component is seen to be only a small percentage of the power expended within the cilia layer. Therefore the rate of total energy expenditure for propulsion may be expected to depend primarily on the configuration of ciliary movement within the cilia layer rather than on the body shape. These conclusions may partially explain the occurrence of a great variety of shapes for ciliated creatures, and may indicate that this manner of locomotion affords an evolutionary advantage.

Another feature predicted by the model is a vast difference in the streamlines for the translation of an inert impermeable body and a freely swimming micro-organism of the same shape. Qualitatively, good agreement is found between the theoretically predicted streamlines and experimental streak photographs of freely swimming and inert sedimenting micro-organisms.

It is hoped that the present investigation will serve to lay the groundwork for further improvement of the model that will enhance its versatility and accuracy in application to the phenomena of ciliary propulsion. As an initial step in this regard, one might consider more generalized boundary conditions in order to facilitate a matching of the exterior flow field to any suitable model for the flow within the cilia layer. We note that recently, in a separate approach, Brennen (1975) has considered a similar geometry in which an exterior flow field equivalent to the present solution was matched to an envelope model. While the results of this analysis are not without merit, in view of the limitations of the envelope model it would be of interest to consider a treatment in which the flow in the vicinity of the cilia layer were represented more accurately. Here the singularity methods for Stokes flows may play a significant role. A further improvement, which would be of practical value in the laboratory, would be to consider the effect of proximity of the organism to walls.

Appendix. Evaluation of the rate of energy dissipation

In this appendix we evaluate (38), which may be written as

$$\dot{E} = \dot{E}_p + \dot{E}_\tau, \tag{56}$$

where

$$\dot{E}_p = \int_S (p\mathbf{n}).\mathbf{u}^l\, dS, \quad \dot{E}_\tau = -\int_S (\boldsymbol{\tau}\mathbf{n}).\mathbf{u}^l\, dS, \tag{57), (58}$$

and $\boldsymbol{\tau}$ is the viscous stress tensor given by

$$\boldsymbol{\tau} = \mu[(\nabla \mathbf{u}) + (\nabla \mathbf{u})^{\mathrm{T}}], \tag{59}$$

with T indicating the transpose. We note that an element of surface area of the prolate spheroid is given by

$$dS = 2\pi(1-e^2)^{\frac{1}{2}}(a^2 - e^2z^2)^{\frac{1}{2}}\,dz \quad (-a \leqslant z \leqslant a). \tag{60}$$

From (19) and (21) it is easily found that the pressure on the surface S is

$$p_0 = -4\mu\alpha e z/(a^2 - e^2z^2) \quad (-a \leqslant z \leqslant a). \tag{61}$$

Employing (61), (60), (23), (7) and (3), we have for (57)

$$\dot{E}_p = -8\pi\mu\alpha e(1-e^2)\left[-2\alpha L + \beta\left(\frac{4e}{1-e^2} - 2L\right)\right]\int_{-a}^{a} \frac{z^2\,dz}{a^2 - e^2z^2}. \tag{62}$$

The integral may be readily evaluated to yield

$$\dot{E}_p = 16\pi\mu a(2e - L)\,e^{-2}\{-\alpha^2(1-e^2)\,L + [2e - (1-e^2)\,L]\,\alpha\beta\}. \tag{63}$$

To evaluate (58) it is convenient to express the velocity field in terms of prolate-spheroidal co-ordinates (ξ, η, ϕ) defined by the transformation

$$z + i\rho = c\cosh(\xi + i\eta) \quad (0 < \xi < \infty,\ 0 < \eta < \pi,\ c > 0). \tag{64}$$

For convenience we define

$$\tau = \cosh\xi, \quad \zeta = \cos\eta \quad (1 < \tau < \infty,\ -1 \leqslant \zeta \leqslant 1). \tag{65}$$

From (64) and (65) it is found that

$$\rho = c(\tau^2 - 1)^{\frac{1}{2}}(1 - \zeta^2)^{\frac{1}{2}}, \quad z = c\tau\zeta. \tag{66}$$

The co-ordinate surface defined by τ = constant is a prolate spheroid whose eccentricity is given by $e = 1/\tau$ with foci at $z = \pm c$. The unit vector tangential to the τ co-ordinate curve is just $\mathbf{n}$, while the unit vector tangential to the ζ co-ordinate curve is $\mathbf{s}$. Thus we may write for the velocity field

$$\mathbf{u}^l = u_1(\tau, \zeta)\,\mathbf{n} + u_2(\tau, \zeta)\,\mathbf{s}. \tag{67}$$

By substituting $c\tau\zeta$ for z and $1/\tau$ for e into (23), (8) and (7), we obtain after some manipulation

$$u_1 = 2\zeta f/(\tau^2 - \zeta^2)^{\frac{1}{2}}(\tau^2 - 1)^{\frac{1}{2}}, \tag{68}$$

$$u_2 = -(1-\zeta^2)^{\frac{1}{2}} f'/(\tau^2 - \zeta^2)^{\frac{1}{2}}, \tag{69}$$

where

$$f = 2\beta\tau + (\alpha + \beta)(1 - \tau^2)\log\left(\frac{\tau+1}{\tau-1}\right) \tag{70}$$

and a prime denotes differentiation with respect to τ. In prolate-spheroidal co-ordinates the integrand in (58) may be expressed as (see, for example, Happel & Brenner 1973)

$$\begin{aligned}\{[(\nabla \mathbf{u}) + (\nabla \mathbf{u})^{\mathrm{T}}]\,\mathbf{n}\}.\mathbf{u}^l = &-2u_1 h\left[\frac{\partial u_1}{\partial q_1} + hu_2\frac{\partial}{\partial q_2}\left(\frac{1}{h}\right)\right] \\ &- u_2 h\left[\frac{\partial u_2}{\partial q_1} - hu_1\frac{\partial}{\partial q_2}\left(\frac{1}{h}\right) + \frac{\partial u_1}{\partial q_2} - hu_2\frac{\partial}{\partial q_1}\left(\frac{1}{h}\right)\right],\end{aligned} \tag{71}$$

where $q_1 = \xi$, $q_2 = \eta$ and h is the metric coefficient $1/c(\sinh^2\xi + \sin^2\eta)^{\frac{1}{2}}$. In terms of τ and ξ we note that

$$\frac{\partial}{\partial q_1} = (\tau^2-1)^{\frac{1}{2}}\frac{\partial}{\partial \tau}, \quad \frac{\partial}{\partial q_2} = -(1-\zeta^2)^{\frac{1}{2}}\frac{\partial}{\partial \zeta} \tag{72}$$

and

$$h = 1/c(\tau^2-\zeta^2)^{\frac{1}{2}}. \tag{73}$$

Furthermore, an element of surface area is given by (cf. Happel & Brenner)

$$dS = -2\pi c^2(\tau^2-\zeta^2)^{\frac{1}{2}}(\tau^2-1)^{\frac{1}{2}}\,d\zeta \quad (-1 \leqslant \zeta \leqslant 1). \tag{74}$$

Equation (58) may now be evaluated by employing (68)–(74). This calculation is lengthy but straightforward and involves only some elementary integrals. Upon evaluating the result on the particular prolate spheroid $\tau = 1/e$, we find, after considerable algebraic manipulation, that

$$\begin{aligned}\dot{E}_\tau = 8\pi\mu a\{&\{2(e^2-3)+[(7-2e^2-e^4)e^{-1}]L+[-2(1-e^2)e^{-2}]L^2\}\alpha^2\\ &+\{-8(1-e^2)+[4(2-2e^2-e^4)e^{-1}]L+[-2(1-e^2)e^{-2}]L^2\}\alpha\beta\\ &+\{-8e^4(1-e^2)^{-1}+[4e^3(1+e^2)(1-e^2)^{-1}]L\}\beta^2\}.\end{aligned} \tag{75}$$

The addition of (75) and (63) yields (41).

REFERENCES

BATCHELOR, G. K. 1967 *An Introduction to Fluid Dynamics*. Cambridge University Press.

BLAKE, J. R. 1971*a* A spherical envelope approach to ciliary propulsion. *J. Fluid Mech.* **46**, 199–208.

BLAKE, J. R. 1971*b* Infinite models for ciliary propulsion. *J. Fluid Mech.* **49**, 209–222.

BLAKE, J. R. 1972 A model for the micro-structure in ciliated organisms. *J. Fluid Mech.* **55**, 1–23.

BLAKE, J. R. 1973 A finite model for ciliated micro-organisms. *J. Biomech.* **6**, 133–140.

BLAKE, J. R. & SLEIGH, M. A. 1974 Mechanics of ciliary locomotion. *Biol. Rev.* **49**, 85–125.

BRENNEN, C. 1974 An oscillating-boundary-layer theory for ciliary propulsion. *J. Fluid Mech.* **65**, 799–824.

BRENNEN, C. 1975 Hydromechanics of propulsion for ciliated micro-organisms. In *Swimming and Flying in Nature*, vol. 1 (ed. T. Y. Wu, C. Brennen & C. Brokaw), pp. 235–251. Plenum.

CHWANG, A. T. & WU, T. Y. 1974 A note on potential flow involving prolate spheroids. *Schiffstech.* **21**, 19–31.

CHWANG, A. T. & WU, T. Y. 1975 Hydromechanics of low-Reynolds-number flow. Part 2. Singularity method for Stokes flows. *J. Fluid Mech.* **67**, 781–815.

HAPPEL, J. & BRENNER, H. 1973 *Low Reynolds Number Hydrodynamics*. Nordhoff.

HIRAMOTO, Y. 1974 Mechanics of ciliary movement. In *Cilia and Flagella* (ed. M. A. Sleigh), pp. 177–196. Academic.

KELLER, S. R. 1975 Fluid mechanical investigations of ciliary propulsion. Ph.D. thesis, California Institute of Technology.

KELLER, S. R., WU, T. Y. & BRENNEN, C. 1975 A traction-layer model for ciliary propulsion. In *Swimming and Flying in Nature*, vol. 1 (ed. T. Y. Wu, C. Brennen & C. Brokaw), pp. 253–272. Plenum.

LAMB, H. 1932 *Hydrodynamics*. Cambridge University Press.

LIGHTHILL, M. J. 1952 On the squirming motion of nearly spherical deformable bodies through liquids at very small Reynolds numbers. *Comm. Pure Appl. Math.* **5**, 109–118.

SLEIGH, M. A. 1969 Coordination of the rhythm of beat in some ciliary systems. *Int. Rev. Cytol.* **25**, 31–54.

SLEIGH, M. A. & HOLWILL, M. E. J. 1969 Energetics of ciliary movement in *Sabellaria* and *Mytilus*. *J. Exp. Biol.* **50**, 733–743.

TAYLOR, G. I. 1951 Analysis of swimming of microscopic organisms. *Proc. Roy. Soc.* A **209**, 447–461.

YONEDA, M. 1962 Force exerted by a single cilium of *Mytilus edulis*. *J. Exp. Biol.* **39**, 307–317.

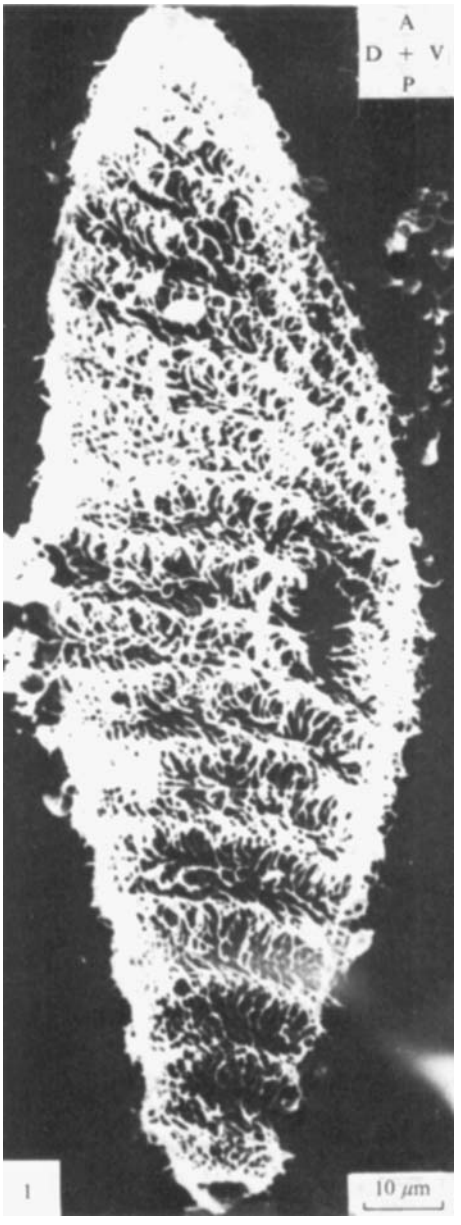

FIGURE 1. Scanning electron micrograph of *Paramecium multimicronucleatum*. (Courtesy S. L. Tamm.)

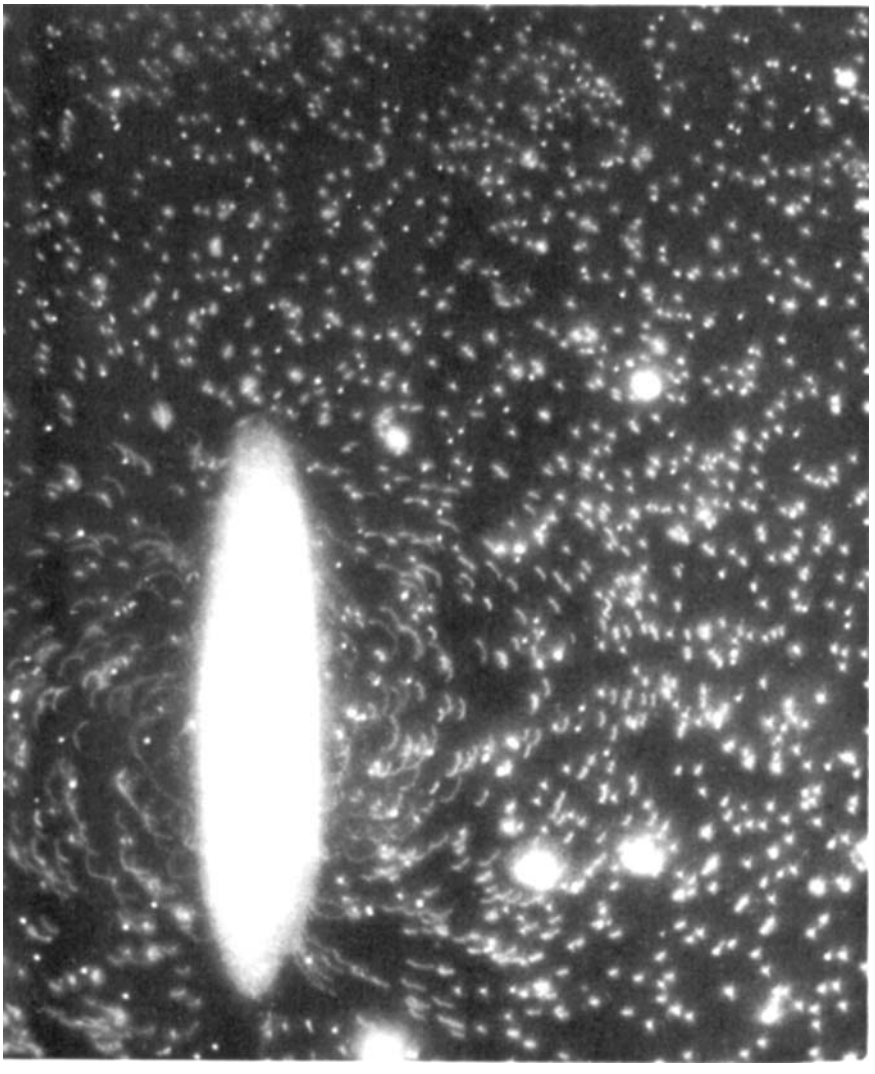

FIGURE 9. Streak photograph of a freely swimming *Paramecium caudatum*.

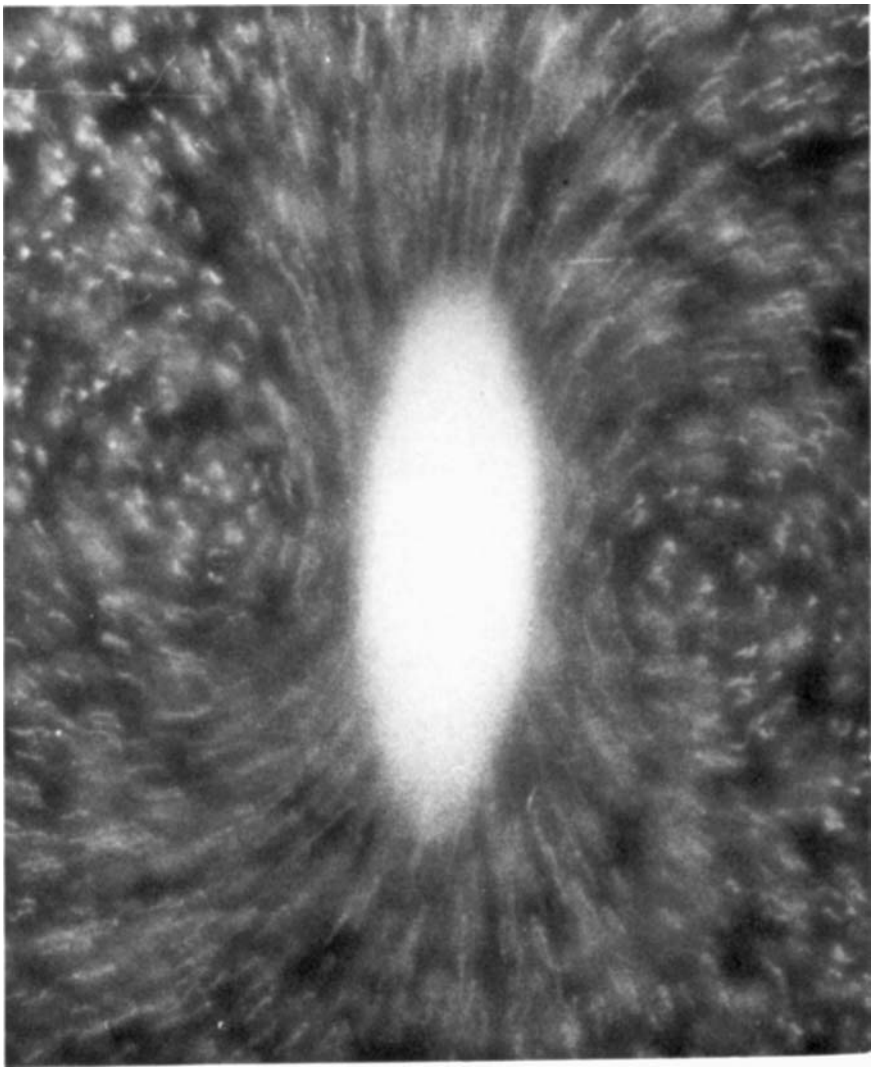

FIGURE 10. Streak photograph of a dead *Paramecium caudatum* falling under the influence of gravity.